Magnetically sensitive light-induced reactions in cryptochrome are consistent with its proposed role as a magnetoreceptor

Kiminori Maeda[a,1], Alexander J. Robinson[a,1], Kevin B. Henbest[a], Hannah J. Hogben[b], Till Biskup[b], Margaret Ahmad[c,d], Erik Schleicher[e], Stefan Weber[e], Christiane R. Timmel[a,2], and P. J. Hore[b,2]

[a]Department of Chemistry, University of Oxford, Centre for Advanced Electron Spin Resonance, Inorganic Chemistry Laboratory, Oxford OX1 3QR, United Kingdom; [b]Department of Chemistry, University of Oxford, Physical and Theoretical Chemistry Laboratory, Oxford OX1 3QZ, United Kingdom; [c]Université Paris VI, 4 Place Jussieu, 75005 Paris, France; [d]Pennsylvania State University, Media, PA 19063; and [e]Institute of Physical Chemistry, Albert-Ludwigs-Universität Freiburg, 79104 Freiburg, Germany

Edited by* Nicholas J. Turro, Columbia University, New York, NY, and approved January 27, 2012 (received for review November 17, 2011)

Among the biological phenomena that fall within the emerging field of "quantum biology" is the suggestion that magnetically sensitive chemical reactions are responsible for the magnetic compass of migratory birds. It has been proposed that transient radical pairs are formed by photo-induced electron transfer reactions in cryptochrome proteins and that their coherent spin dynamics are influenced by the geomagnetic field leading to changes in the quantum yield of the signaling state of the protein. Despite a variety of supporting evidence, it is still not clear whether cryptochromes have the properties required to respond to magnetic interactions orders of magnitude weaker than the thermal energy, k_BT. Here we demonstrate that the kinetics and quantum yields of photo-induced flavin—tryptophan radical pairs in cryptochrome are indeed magnetically sensitive. The mechanistic origin of the magnetic field effect is clarified, its dependence on the strength of the magnetic field measured, and the rates of relevant spin-dependent, spin-independent, and spin-decoherence processes determined. We argue that cryptochrome is fit for purpose as a chemical magnetoreceptor.

magnetic compass | magnetoreception | migratory birds | quantum biology | radical pair mechanism

Originally identified in plants (1), and subsequently found in organisms ranging from bacteria to insects and mammals, cryptochromes are blue-light photoreceptor proteins with a variety of functions including entrainment of circadian rhythms and, in plants, light-dependent regulation of growth and development [reviewed in Ref. (2)]. They have high sequence-homology and structural similarity to their evolutionary ancestors, the DNA photolyases (3, 4) and all members of the cryptochrome/photolyase family contain the redox-active cofactor flavin adenine dinucleotide (FAD). Cryptochromes were proposed as potential magnetoreceptors by Ritz et al. in 2000 in an attempt to explain the mechanism by which migratory birds are able to sense the direction of the Earth's magnetic field for the purpose of navigation (5). Based on an earlier suggestion by Schulten (6), and drawing on the known magnetic sensitivity of radical-pair reactions in vitro [reviewed in Ref. (7)], this idea has gained considerable support. Eleven years after the original suggestion, cryptochrome remains the only candidate radical-pair magnetoreceptor.

Photoreduction of the fully oxidized state of FAD in most proteins of the cryptochrome/photolyase family appears to be mediated by electron transfer along a conserved triad of tryptophan (Trp) residues to give a flavosemiquinone radical, $FAD^{\bullet-}$ or $FADH^{\bullet}$, together with a radical derived from the terminal residue of the Trp-triad (8–11) (Fig. 1). At least in plants, where the photo-active functions of cryptochromes are best understood, the flavosemiquinone form of the protein is thought to be the signaling state (12, 13). If the quantum yield of this state were dependent on the direction of the Earth's magnetic field, then in principle cryptochrome could act as a compass sensor. The evidence accumulated over the last 11 years in support of the cryptochrome hypothesis has been reviewed in Refs. (14, 15). Hitherto, cryptochrome photochemistry has not been shown to be magnetically sensitive.

Cryptochromes have also attracted attention as potential mediators of biological effects of extremely low frequency (ELF) electromagnetic fields. Five observations are pertinent here. (*i*) Epidemiology suggests a weak association between increased risks of childhood leukemia and long-term exposure to 50/60 Hz ELF fields stronger than 0.4 μT (16, 17). On this evidence, the International Agency for Research on Cancer (a part of the World Health Organization) has classified ELF magnetic fields as "possibly carcinogenic to humans" (18). The UK National Radiological Protection Board (now the Health Protection Agency), however, concluded in 2001 that there was no compelling evidence for carcinogenicity (19). (*ii*) Disruption of circadian timing has been associated with susceptibility to cancer (20). (*iii*) Cryptochromes are key components in the transcriptional regulation of mammalian circadian clocks (although there is no evidence that they function as photoreceptors or for the involvement of radicals) (2). (*iv*) The radical-pair mechanism is currently the only physically plausible mechanism by which magnetic interactions that are orders of magnitude weaker than k_BT can affect chemical reactions (7, 21). (*v*) Of the various radical-pair systems considered as possible mediators of biological magnetic-field effects, cryptochromes are the most likely candidates given their known (photo-)chemical and physical properties (22).

In the following, we demonstrate that photo-induced radical pairs in a cryptochrome (Cry-1 from the plant *Arabidopsis thaliana*, *At*Cry) *are* sensitive in vitro to weak applied magnetic fields. Comparing the behavior of *At*Cry with that of *Escherichia coli* photolyase (*Ec*PL), we determine the reaction steps responsible for the magnetic-field effect, elucidate what appears to be the principal spin-decoherence mechanism, obtain estimates of the rates of these processes, and provide evidence that radical pairs in cryptochromes could have the properties required to respond to Earth-strength (approximately 50 μT) fields at physiological temperatures.

Author contributions: C.R.T. and P.J.H. designed research; K.M., A.J.R., and K.B.H. performed research; K.M., A.J.R., K.B.H., H.J.H., T.B., E.S., S.W., C.R.T., and P.J.H. discussed the data; M.A., E.S., and S.W. expressed the proteins; K.M., A.J.R., K.B.H., H.J.H., T.B., C.R.T., and P.J.H. analyzed data; and P.J.H. wrote the paper.

The authors declare no conflict of interest.

*This Direct Submission article had a prearranged editor.

[1]These authors contributed equally to this work.

[2]To whom correspondence may be addressed. E-mail: peter.hore@chem.ox.ac.uk or christiane.timmel@chem.ox.ac.uk.

This article contains supporting information online at www.pnas.org/lookup/suppl/doi:10.1073/pnas.1118959109/-/DCSupplemental.

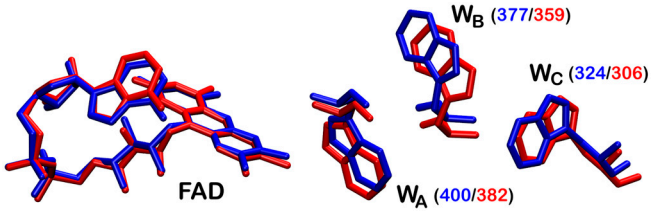

Fig. 1. The electron transfer pathway leading from the protein surface to the FAD cofactor buried within the protein. Shown are the relative positions of the FAD cofactor and the Trp-triad (W_A, W_B, W_C) in *At*Cry [blue, PDB entry 1U3D (37)] and *Ec*PL [red, PDB entry 1DNP (48)]. The proposed magnetically sensitive species comprises a radical derived from the FAD and one from the terminal tryptophan residue, W_C (Trp-324 in *At*Cry; Trp306 in *Ec*PL). The center-to-center distance between the tricyclic isoalloxazine ring system of FAD and the indole group of W_C is 1.90 nm in *At*Cry (37).

Results

Magnetic-Field Effect on Radical-Pair Kinetics. The photochemistry of *At*Cry and *Ec*PL has been studied using flash photolysis transient absorption spectroscopy. Figs. 2 *A* and *C* show difference spectra obtained from *At*Cry and *Ec*PL containing the flavin chromophore in its fully oxidized state, in (liquid) water-glycerol mixtures in the absence of an applied magnetic field. The two sets of spectra are broadly similar, showing depletion of the FAD ground state at 450 nm and formation of FAD and Trp radicals, visible as overlapping bands at wavelengths below 420 nm and above 500 nm. The principal differences between the two proteins are the relatively rapid (approximately 10 μs) attenuation of the signal below 420 nm for *At*Cry and the change in the shape of the signal in the range 500–650 nm for *Ec*PL (also approximately 10 μs).

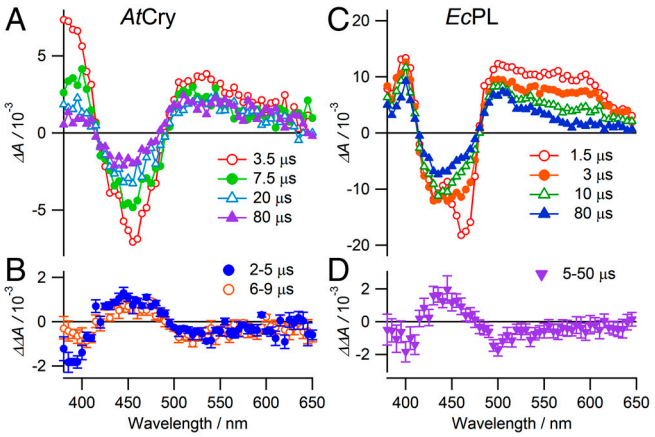

Fig. 2. Transient absorption spectra and magnetic-field action spectra of *At*Cry and *Ec*PL. Transient absorption spectra, $\Delta A(0)$, of (*A*) *At*Cry and (*C*) *Ec*PL. $\Delta A(0)$ is the difference between signals recorded with and without a 460 nm, 5 ns pump light pulse in the absence of an applied magnetic field. The spectra were integrated over 1 μs periods centered at the indicated times after the pump pulse. Each spectrum is the average of two transients. The laser repetition rate was kept low (0.05 Hz) to minimize protein photodegradation. The 1.5 μs signal in (*C*) at 460 nm is distorted by a transient effect of the laser pulse on the photomultiplier detector. Experimental conditions: *At*Cry, 250 K, 60% (v/v) glycerol solution; *Ec*PL, 250 K, 50% (v/v) glycerol solution. (*B*) and (*D*) Magnetic-field action spectra of *At*Cry and *Ec*PL, respectively, recorded under the same conditions as (*A*) and (*C*), presented as $\Delta\Delta A = \Delta A(28\ \text{mT}) - \Delta A(0)$. Two transients were recorded with the magnetic field and two without. At each wavelength the double-difference kinetic time profiles were smoothed with a 2 μs boxcar function and the mean and standard deviation calculated over the indicated time intervals. At each wavelength the mean ± standard deviation is plotted. The minor differences between the data shown in (*C*) and (*D*) and the data reported by Henbest et al. (23) are attributed to the different experimental conditions of the latter: 278 K, 20% (v/v) glycerol, 5 mM potassium ferricyanide.

The spectra of *Ec*PL in Fig. 2*C* and those obtained at higher temperatures and lower glycerol contents are consistent with rapid (≪1 μs) formation, by photo-induced electron transfer, of a [$FAD^{\bullet-}TrpH^{\bullet+}$] radical pair followed by deprotonation of the $TrpH^{\bullet+}$ radical (approximately 10 μs) to give the neutral $Trp^{\bullet}$ radical (23). Simultaneously, the ground state band at 450 nm recovers with an approximately 10 μs component via electron–hole recombination of [$FAD^{\bullet-}TrpH^{\bullet+}$] to regenerate the FAD and TrpH ground states. Henceforth we refer to the sequentially formed radical pairs, [$FAD^{\bullet-}TrpH^{\bullet+}$] and [$FAD^{\bullet-}Trp^{\bullet}$] in *Ec*PL, as RP1 and RP2, respectively.

The situation is a little more complex for *At*Cry. The spectra in Fig. 2*A* are consistent with the rapid initial formation and slower recombination of [$FAD^{\bullet-}TrpH^{\bullet+}$] (RP1) and the subsequent formation of a secondary radical pair (RP2), the identity of which is less clear than for *Ec*PL. The tryptophanyl radical in *At*Cry deprotonates either fully or partially; both are consistent with the data. The absorption decay observed below 420 nm indicates either protonation of $FAD^{\bullet-}$ to give the neutral $FADH^{\bullet}$ radical or the disappearance of a tyrosyl radical formed very rapidly (<1 μs) by electron transfer from a nearby tyrosine residue: $TrpH^{\bullet+} + Tyr \rightarrow TrpH + Tyr^{\bullet+}$. Protonation of $FAD^{\bullet-}$ in an algal cryptochrome has been observed on the same timescale as the spectral changes in Fig. 2*A* (24); the marked drop in absorption below 420 nm (time constant, approximately 2 μs) was found to be accompanied by a smaller rise between 500 and 600 nm. The latter is not seen here probably because it is obscured by the recombination of RP1 which appears to be faster in *At*Cry than in the algal protein. Formation of tyrosyl radicals has been reported in *At*Cry (9, 10) and in two photolyases (25, 27), but, at least for *At*Cry, on a much slower (approximately 1 ms) timescale (9) than the changes in Fig. 2*A* which, if due to a tyrosyl radical, would have to be assigned to its reduction by an unknown electron donor following its formation at an unprecedented fast rate. We therefore conclude that RP2 in *At*Cry is most likely to be formed from RP1 by $FAD^{\bullet-}$ protonation. We stress that the identity of RP2 in *At*Cry is not crucial for the interpretation of the magnetic-field effects reported below. In light of previous work (9, 10, 24, 28, 29), the Trp radicals are presumed to come from the terminal residue of the Trp-triad, i.e. Trp-324 in *At*Cry and Trp-306 in *Ec*PL.

Figs. 2 *B* and *D* show the changes in the transient absorption spectra of *At*Cry and *Ec*PL, respectively, resulting from the application of a 28 mT magnetic field. Broadly similar to one another, and mirroring the shapes of Figs. 2 *A* and *C*, respectively, these action spectra show that the applied field reduces the transient yields of both FAD and Trp radicals and enhances the recovery of the FAD ground state. The difference between the 2–5 μs and 6–9 μs data below 400 nm in Fig. 2*B* is consistent with the $FAD^{\bullet-} \rightarrow FADH^{\bullet}$ protonation reaction (23).

Insight into the origin of the magnetic sensitivity is provided by the transient absorption kinetics. Typical time profiles are shown in Fig. 3, recorded for *At*Cry and *Ec*PL at a wavelength where $FAD^{\bullet-}$, $FADH^{\bullet}$, $TrpH^{\bullet+}$ and $Trp^{\bullet}$ radicals all have significant absorptions. Fig. 3*A* shows a rapid (1.2 μs) initial drop in absorption resulting from the recombination of RP1 and its transformation into RP2, followed by a much slower (>100 μs) decay arising from the recombination of RP2 and any other processes that return these radicals to their diamagnetic precursors. *Ec*PL exhibits a similar biphasic behavior (Fig. 3*C*, time constants 2.5 μs and >100 μs) with the faster component again attributable to RP1 recombination and RP1 → RP2 conversion ($TrpH^{\bullet+}$ deprotonation). As seen in Figs. 3 *B* and *D*, the effect of the magnetic field is predominantly on the initial fast phase (i.e., during the lifetime of RP1) and leads to a 10–20% suppression of the yield of RP2.

Photochemical Reaction Mechanism. The magnetic responses of both *At*Cry and *Ec*PL are consistent with the reaction schemes

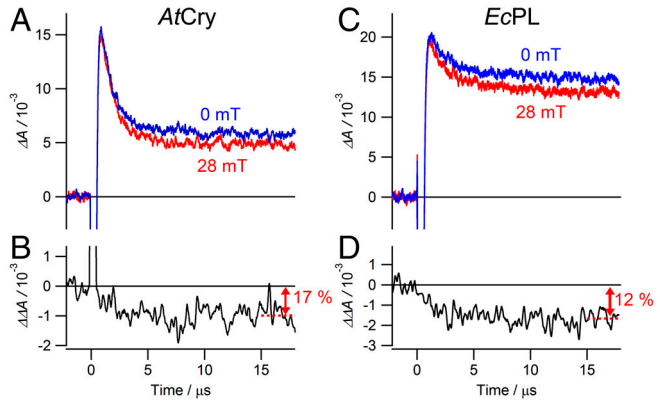

Fig. 3. Magnetic-field effects on the photochemical kinetics of *At*Cry and *Ec*PL. Transient absorption kinetic time profiles of (*A*) *At*Cry and (*C*) *Ec*PL both recorded at 510 nm with and without a 28 mT applied magnetic field. (*B*) and (*D*) Differences between the two signals shown in (*A*) and in (*C*), respectively: $\Delta\Delta A = \Delta A(28\ \mathrm{mT}) - \Delta A(0)$. 200 ns boxcar smoothing was used to produce (*B*) and (*D*); no smoothing was used for (*A*) and (*C*). Experimental conditions: *At*Cry, 270 K in 60% (v/v) glycerol solution; *Ec*PL, 250 K in 50% (v/v) glycerol solution. Similar traces for both proteins were observed at temperatures between 240 K and 275 K and glycerol contents between 25% and 65% (*SI Appendix*).

in Fig. 4. RP1 interconverts coherently between singlet and triplet states under the influence of magnetic interactions internal to the radicals (electron-nuclear hyperfine couplings) and Zeeman interactions with the external magnetic field. Only the singlet state of RP1 can revert to the ground state (FAD + TrpH) by electron-hole recombination, the corresponding reaction of the triplet state being spin-forbidden. Simultaneously, one of the constituents of RP1 changes its protonation state to give RP2, a process that is not subject to spin-selection rules and which singlet and triplet undergo at equal rates. The applied magnetic field alters the time-dependent probability that RP1 is singlet or triplet and so changes the fractions of radical pairs that proceed along the two competing pathways. The nonequilibrium state of the spin system allows magnetic interactions much weaker than $k_B T$ to alter the reaction yields. As indicated by the transient absorption data (Figs. 2 and 3), the RP1 reactions occur on a 10 µs timescale; i.e., slow enough to allow time for a 50 µT magnetic field to modify the singlet-triplet interconversion and fast enough to compete with spin-decoherence, which has been shown by time-resolved EPR to occur in approximately 10 µs (11). Experimental evidence that RP1 is formed in a *singlet* state from the photo-excited singlet state of the FAD cofactor (^{1}FAD*) is discussed in the *SI Appendix*.

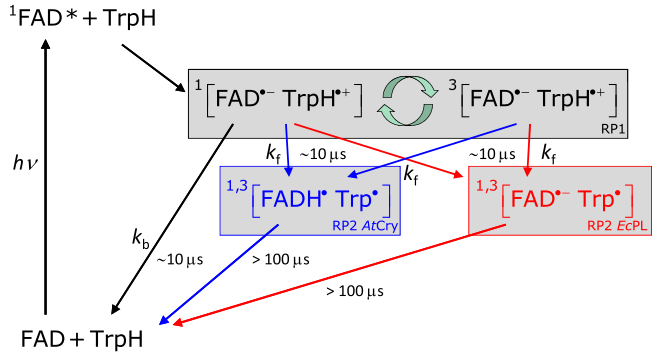

Fig. 4. Proposed photochemical reaction schemes for *At*Cry and *Ec*PL. The black arrows and species are common to both proteins; the blue and red features refer to *At*Cry and *Ec*PL, respectively. k_b and k_f are first-order rate constants for electron–hole recombination of RP1 and formation of RP2 from RP1, respectively. Although RP2 in *At*Cry is here drawn as [FADH•Trp•], the protonation state of the Trp radical is not certain. The curved green arrows indicate the coherent, magnetic field-dependent interconversion of the singlet and triplet states of RP1.

Kinetic Regulation of Magnetic Responses. The changes in the photochemical kinetics of *At*Cry and *Ec*PL reported above are produced by applied magnetic fields some 500 times stronger than the Earth's field. To shed light on the conditions under which cryptochrome might be sensitive to much weaker fields, we have sought to clarify some of the factors that determine the amplitude of the responses at 28 mT.

A 28 mT magnetic field elicits 10–20% changes in the yield of RP2 in both *At*Cry and *Ec*PL (Fig. 3), substantially larger than the 3–4% effects previously reported for *Ec*PL in a solution with a lower glycerol content (23). A possible explanation for this difference can be found in the earlier observation (30) that the deprotonation rate (k_f) of the terminal TrpH$^{\bullet+}$ radical in *Ec*PL decreases with increasing concentration of glycerol, an effect attributed to release of the proton to the solvent. Changes in k_f alter the competition between the k_b and k_f reactions (Fig. 4) and so have the potential to tune the magnetic-field effect. As shown in Fig. 5 for *Ec*PL, both the lifetime of RP1 (determined by the k_b and k_f steps, Fig. 4) and the magnetic-field effect on the quantum yield of RP2 increase with increasing glycerol concentration and decreasing temperature, with an approximately linear correlation between the two quantities. We comment on the origin of this effect in the *SI Appendix*.

Magnetic-field Dependence of Radical Yields. Effects of magnetic fields substantially weaker than 28 mT have been explored for *At*Cry and *Ec*PL; the results are shown in Fig. 6. The fractional change in the yield of RP2 (as measured at 510 nm) is given for magnetic fields down to about 1 mT. The changes are roughly three times stronger for *At*Cry than for *Ec*PL but otherwise rather similar. Above 5 mT, both proteins show typical radical-pair behavior (7): a monotonic increase in the magnitude of the effect, leveling off in both cases at magnetic fields stronger than about 25 mT. The comparatively large asymptotic magnetic-field effects (>20% for *At*Cry and >8% for *Ec*PL) observed here are assumed to arise from the relatively long lifetime of the protein-bound radicals and the restrictions placed on their dynamics by the protein environment.

The width of such field-profiles is often characterized by the parameter $B_{\frac{1}{2}}$, the magnetic field at which the effect reaches half

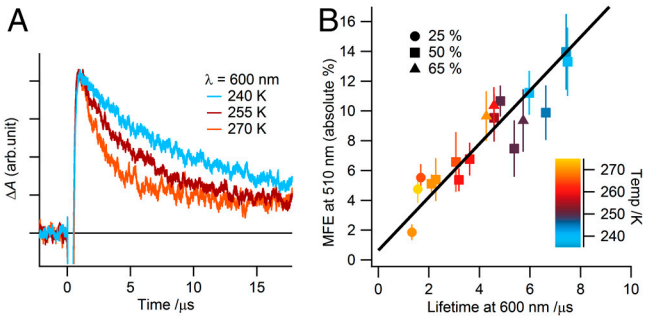

Fig. 5. Correlation between the magnetic-field effect on the yield of RP2 and the lifetime of RP1 in *Ec*PL. (*A*) Transient absorption kinetic time profiles of *Ec*PL in 50% (v/v) glycerol solution in the absence of an applied magnetic field at the temperatures indicated. Recorded at 600 nm, these signals reflect the kinetics of the reactions: TrpH$^{\bullet+}$ → Trp$^\bullet$ + H$^+$ and ^{1}[FAD$^{\bullet-}$TrpH$^{\bullet+}$] → FAD + TrpH (Fig. 4). Lifetimes were extracted from such data by fitting to a monoexponential decay with a constant offset. (*B*) Effect of a 28 mT magnetic field on the yield of RP2 (recorded at 510 nm) plotted against the lifetime of RP1 (measured at 600 nm) over a range of temperatures and glycerol concentrations, as indicated. The vertical axis is the absolute value of the fractional magnetic-field effect (MFE): $|\Delta A(28\ \mathrm{mT}) - \Delta A(0)|/\Delta A(0)$. The data plotted here are given in the *SI Appendix*.

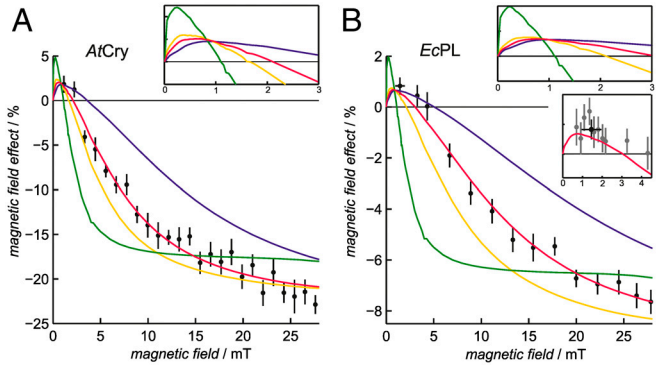

Fig. 6. Magnetic field-dependence of the yield of RP2 in *At*Cry and *Ec*PL. The percentage change in the yield of RP2 (measured at 510 nm) as a function of the strength of the applied magnetic field for (*A*) *At*Cry and (*B*) *Ec*PL. Experimental conditions: (*A*) *At*Cry, 60% glycerol, 270 K; (*B*) *Ec*PL, 50% glycerol, 260 K. The red lines are the best-fit simulations obtained using the singlet-triplet dephasing model described in the text, with $k_f = 2.5 \times 10^5\ s^{-1}$ and (*A*) $k_b = 4.9 \times 10^5\ s^{-1}$, $k_{STD} = 1.1 \times 10^7\ s^{-1}$; (*B*) $k_b = 1.2 \times 10^5\ s^{-1}$, $k_{STD} = 2.7 \times 10^7\ s^{-1}$. The other lines are simulations with the same values of k_f and k_b but (*A*) $k_{STD}/s^{-1} = 0$ (green), 5×10^6 (yellow), 5×10^7 (blue); (*B*) $k_{STD}/s^{-1} = 0$ (green), 1×10^7 (yellow), 1×10^8 (blue). The two larger insets show expanded views of the simulations in the low field region. The irregularities visible in some of these curves arise from energy-level anticrossings. The smaller inset in (*B*) shows, on an expanded scale, the best-fit simulation together with 8 measurements in the range 0.7–2.2 mT that were averaged to obtain the (black) point plotted at $B = 1.5$ mT in this inset and in the main panel. The error bars associated with this data point represent ± one standard deviation of the eight measurements. Each data point in the main panels is the average of (*A*) 10 and (*B*) 40 (>3 mT) or 80 (<3 mT) transients. At each applied magnetic-field strength *B*, the double-difference kinetic time profiles $\Delta A(B) - \Delta A(0)$ were smoothed with (*A*) 5 μs and (*B*) 0.5 μs boxcar functions. The mean ± standard deviation (calculated over the time intervals: (*A*) 2–170 μs and (*B*) 7–15 μs is plotted for each datum.

its limiting size at high field. Using hyperfine coupling data for $FAD^{\bullet-}$ and $TrpH^{\bullet+}$, the Weller equation (31) gives an estimate for $B_{\frac{1}{2}}$ of approximately 3 mT for RP1 (see *SI Appendix*). The observed values of $B_{\frac{1}{2}}$ (Fig. 6) are substantially larger: around 10–12 mT for both proteins. Discrepancies of this kind occur quite commonly for radical-pair reactions and have often been attributed to electron spin-decoherence within the radical pair (see below) (32, 33). Also visible in Fig. 6 are indications that for both proteins the phase of the magnetic response inverts for magnetic fields weaker than 2–3 mT. We return to this point below.

Reversible Electron Transfer in the Trp Triad. The theoretical basis of the radical-pair mechanism is sufficiently developed that quantitative interpretation of experimental data has become fairly routine especially when, as here, the separation and relative orientation of the two radicals are constrained. Even though the data in Fig. 6 exhibit little structure, successful numerical simulations may supply insights into the decoherence mechanism(s) responsible for the larger than expected $B_{\frac{1}{2}}$ values.

Reversible electron transfer between the distal and intermediate residues of the Trp triad has the potential to increase the observed $B_{\frac{1}{2}}$. Denoting the proximal, intermediate and distal tryptophans as W_A, W_B, and W_C, the electron transport chain may be written:

$$^1FAD^*W_AW_BW_C \rightarrow FAD^{\bullet-}W_A^{\bullet+}W_BW_C \rightarrow \underbrace{FAD^{\bullet-}W_AW_B^{\bullet+}W_C}_{RP0} \underset{k'_{ET}}{\overset{k_{ET}}{\rightleftharpoons}} \underbrace{FAD^{\bullet-}W_AW_BW_C^{\bullet+}}_{RP1}$$

where k_{ET} and k'_{ET} are the rate constants for interconversion of RP1 and the intermediate radical pair comprising $FAD^{\bullet-}$ and $W_B^{\bullet+}$, which we shall call RP0. The limited evidence available suggests that the Trp radical is mostly localized on W_C (i.e., $k_{ET} \gg k'_{ET}$) and that k'_{ET} may be fast enough to allow reversible electron hopping from and to W_B during the lifetime of RP1 (26, 34, 35). Using center-to-center FAD-Trp separations calculated (36) from the X-ray structure of *At*Cry (37) (1.32 nm for RP0 and 1.90 nm for RP1), the interradical electron exchange interactions have been estimated (36) as $|J_{RP0}| \approx 10^3$ mT and $|J_{RP1}| \approx 10^{-1}$ mT. Since $|J_{RP0}|$ greatly exceeds $|J_{RP1}|$, the hyperfine interactions and the magnetic-field strength, electron hopping would cause strong modulation of the exchange interaction resulting in rapid relaxation of singlet-triplet coherences in RP1 (33). The time required for such decoherence is on the order of $(J_{RP0})^{-1}$; i.e., approximately 10 ps. Therefore, if k_{ET} is not much larger than $10^{11}\ s^{-1}$, every time RP1 is converted into RP0 there would be significant decoherence before the electron jumped back. Under these conditions, the singlet-triplet dephasing (STD) rate, k_{STD}, should be close to k'_{ET}.

Standard techniques of quantum spin dynamics (7) were employed to simulate the magnetic-field effects shown in Fig. 6, using the reaction scheme in Fig. 4. Just two (field-independent) variable parameters were used for each protein: k_b and k_{STD}. The rate constant for the RP1 → RP2 reaction was fixed ($k_f = 2.5 \times 10^5\ s^{-1}$) by noting that the magnetic-field effect for *Ec*PL at 28 mT (approximately 8%, Fig. 6*B*) corresponds to a RP1 lifetime of approximately 4 μs (Fig. 5*B*). The same value was used for *At*Cry. In the simulations, all coherent superpositions of a singlet state and a triplet state of RP1 were damped exponentially with the rate constant k_{STD}, and hyperfine couplings were calculated using density functional theory. The red lines in Figs. 6 *A* and *B* are the best-fit simulations, with the optimum parameter values: *At*Cry, $k_b = 4.9 \times 10^5\ s^{-1}$, $k_{STD} = 1.1 \times 10^7\ s^{-1}$; *Ec*PL, $k_b = 1.2 \times 10^5\ s^{-1}$, $k_{STD} = 2.7 \times 10^7\ s^{-1}$. These numbers are plausible: (*i*) A magnetic-field effect as large as approximately 20% requires effective competition between the two reaction pathways, implying $k_b \approx k_f$. (*ii*) RP1 lifetimes with respect to recombination to the ground state (i.e., k_b^{-1}) of approximately 2 μs (*At*Cry) and 8 μs (*Ec*PL) are compatible with the observed transient absorption kinetics. (*iii*) As shown in Fig. 6, the width of the field-dependence is sensitive to the value of k_{STD}; an increase in $B_{\frac{1}{2}}$ from approximately 3 mT to 10–12 mT requires k_{STD} to be substantially larger than k_b and k_f. (*iv*) The value of k_{STD} for *Ec*PL agrees very well with the estimate of k'_{ET} by Popović et al. ($3.2 \times 10^7\ s^{-1}$) (26) but less well with that of Krapf et al. ($1.2 \times 10^4\ s^{-1}$) (35). Simulations in which spin relaxation was omitted (*SI Appendix*), or included by means of other models, were uniformly unsuccessful in accounting for the data shown in Fig. 6 (see *SI Appendix* for details). Additional simulations, also described in the *SI Appendix*, suggest a rationale for the larger magnetic-field effect for *At*Cry compared to *Ec*PL (Fig. 6) and for the correlation shown in Fig. 5.

Sensitivity to Weaker Magnetic Fields. We have shown that the effects of magnetic fields stronger than 5 mT are consistent with singlet-triplet interconversion induced by hyperfine and Zeeman interactions together with singlet-triplet dephasing brought about by electron hopping. In the light of this, we return to the sign change in the magnetic-field effect for both proteins below 2–3 mT (Fig. 6). Such phase inversions have been well documented both theoretically and experimentally in other reaction systems (21, 38, 39) and are usually referred to as "low field effects" (LFE). Numerical simulations of model radical pairs (21) show that when spin relaxation and radical recombination reactions are sufficiently slow, the LFE can be much larger than the 1% effects seen at around 1 mT in Fig. 6, even in much weaker magnetic fields. The best-fit simulations predict LFEs for both proteins with approximately the correct positions and amplitudes. The other simulations in Fig. 6 indicate that as k_{STD} is reduced

the initial slope increases causing the maximum LFE to shift to progressively lower fields. Thus the effect of a 50 μT magnetic field on the yield of RP2 could be significantly larger than implied by the best-fit simulations in Fig. 6 if singlet-triplet dephasing (and any other significant decoherence mechanisms) were sufficiently slow.

Discussion

The cryptochrome hypothesis of radical-pair magnetoreception was proposed 11 years ago. We present here direct evidence that cryptochromes can exhibit the magnetically sensitive photochemistry that is the essential prerequisite for a magnetic compass sensor. Magnetic-field effects on the quantum yields of radicals produced in *At*Cry in viscous solution of about +1% in a 1 mT magnetic field, and about −25% in a 30 mT field, have been detected. The change in phase observed for fields weaker than 2–3 mT is the signature of the low field effect which, under appropriate conditions, could permit significant responses to Earth-strength magnetic fields.

High glycerol concentrations and reduced temperatures have been used here to optimize the observed magnetic responses. One can only speculate about the environment of an avian cryptochrome in a magnetoreceptor cell, but it seems most likely that the proteins would have to be both immobilized and aligned in order to show the anisotropic magnetic responses essential for a compass detection mechanism (5). Restricted molecular motion, leading to slower spin-decoherence, should also be favorable. Both factors prompted our use of mixed aqueous solvents with a higher viscosity than pure water. [Other reasons for using glycerol-water mixtures were (*i*) to regulate the competition between deprotonation of $TrpH^{\bullet+}$ and spin-selective recombination of RP1 in *Ec*PL (Fig. 5); (*ii*) to allow the use of temperatures below 273 K for the same reason; and (*iii*) to stabilize the protein against aggregation and precipitation.] Restricted motion could come about in different and probably more efficient ways in vivo, for example by tethering to membrane proteins or cytoskeletal filaments (40), binding to signaling partners (41–43) and/or cofactors [e.g., ATP (37, 44)], dimerization (45), etc. It does not seem unreasonable to conjecture that under optimum conditions in vivo, the effect of a 50 μT magnetic field could be substantially larger than observed in the present study. Simulations suggest that the low field effect can, under the right conditions, be as large as 10–20% (21). Too little is known about light-dependent cryptochrome signaling in general, and magnetoreception in particular, to say whether this would be large enough to form the basis of a viable magnetoreceptor.

It is evident from our results that a significant magnetic-field effect from a cryptochrome-based radical pair requires kinetic competition on a 1–10 μs timescale, between spin-selective electron-hole recombination, and spin-independent formation of the signaling state. If these processes were much faster than 1 μs there would be insufficient time for the geomagnetic field to influence the spin dynamics; if they were much slower, the effect would almost certainly be attenuated by spin-decoherence (14). It seems unlikely, however, that the conformational changes needed to generate the signaling state [probably rearrangement of the C-terminal domain (46)] could be as fast as 10 μs. Our results show that formation of a secondary species (RP2) from the magnetically sensitive radical pair RP1, $[FAD^{\bullet-}TrpH^{\bullet+}]$, avoids the need for an abnormally rapid protein rearrangement or exceptionally slow spin-decoherence. Protonation of the $FAD^{\bullet-}$ radical (as may occur in *At*Cry) or deprotonation of the $TrpH^{\bullet+}$ radical [as occurs in *Ec*PL (23, 30)] allows the magnetic-field effect on RP1 to be "stored" in the form of a changed quantum yield of the much longer lived state RP2, from which the signaling state can subsequently be generated. The fact that there is no need for the reactions of RP2 to be magnetically sensitive means that its lifetime can greatly exceed its spin-decoherence time without ill effect.

There are now two members of the cryptochrome/photolyase family that show magnetic responses. Given the very different biological functions of *Ec*PL (DNA repair) and *At*Cry (regulation of growth and development, entrainment of circadian rhythms) and the fact that neither bacteria nor plants appear to have specialized magnetoreceptors, we suggest that magnetic sensitivity is a general feature of this protein family and that the results described here may be extrapolated to bird cryptochromes (and possibly even human cryptochromes).

Materials and Methods

Protein Preparation. The expression and purification of *Ec*PL (as a mutant that does not bind the methenyltetrahydrofolate cofactor) are described elsewhere (23, 47). To ensure the FAD cofactor was in its fully oxidized state, the protein was pretreated with potassium ferricyanide as described previously (23). Glycerol was added to approximately 130 μM protein samples in 50 mM Hepes buffer at pH 7.0 with 100 mM KCl to obtain solutions containing 20–50% glycerol (v/v). Unlike our previous study of *Ec*PL (23), potassium ferricyanide was not added to the samples to reoxidize photoreduced flavin.

*At*Cry (full length cryptochrome-1) was expressed in Sf21 cells using a recombinant baculovirus expression vector system and purified by Ni-NTA affinity chromatography. Glycerol was added to approximately 150 μM protein samples in Tris/HCl buffer at pH 7.5 with 500 mM NaCl and 250 mM imidazole to obtain solutions containing 20–60% glycerol (v/v).

Transient Absorption Spectroscopy. Protein samples (approximately 250 μL) were cooled in a cryostat (Oxford Instruments, Optistat CF) with the temperature controlled to within 0.1 K. The sample was held in a quartz cuvette (Hellma 104.002F QS; 10 mm path length, internal dimensions 2 × 10 × 45 mm) at the center of the cryostat. Magnetic-field pulses of approximately 4 ms duration, synchronized with the laser flash, were generated using home-built Helmholtz coils. The maximum magnetic field at the position of the sample was 29 mT. Samples were not shielded from the Earth's magnetic field. Radical pairs in *Ec*PL and *At*Cry were generated by flash photolysis using a dye laser (Sirah Cobra) pumped by a Nd:YAG laser (Continuum Surelite 1). The laser dye was Coumarin 460 (Exciton Inc.) in analytical grade methanol (Fisher Scientific). The Nd:YAG laser produced 5 ns pulses with energy approximately 100 mJ and repetition rate 1 Hz, tuned by means of a Q-switch delay to produce 5–7 mJ, 460 nm pulses (FWHM 37 nm) from the dye laser. Probe light from a 300 W xenon arc lamp (Oriel) was passed through a water filter to cut out infrared components and through long-pass filters to remove unwanted wavelengths and then to the sample in a direction orthogonal to the pump pulses. Pump and probe beams were controlled by mechanical shutters to obtain a 0.05 Hz repetition rate to reduce photodegradation of the light-sensitive samples. Probe light was collected using a monochromator (Oriel 77250), fed into a photomultiplier tube (Hamamatsu R928) and from there to an oscilloscope (Iwatsu-LeCroy Waverunner LT342L). Data were transferred to a personal computer and analyzed using IGOR PRO (Wavemetrics, Inc.) software.

Spin Dynamics Simulations. The magnetic field-dependence of radical-pair reaction yields (Fig. 6) was calculated from the equation of motion of the radical-pair spin density operator in Liouville space including coherent spin dynamics, decoherence processes, and chemical reactivity by means of appropriate superoperators. Singlet-triplet dephasing was introduced as proposed by Shushin (33). Further details are given in the *SI Appendix*.

ACKNOWLEDGMENTS. We thank S. M. Lea, J. Lillington and A. Bowen for discussions and N. Baker and P. Stehle for technical assistance. P.J.H. and C.R.T. were supported by the Electromagnetic Fields Biological Research Trust, the Defense Advanced Research Projects Agency (QuBE: N66001-10-1-4061), and the Engineering and Physical Sciences Research Council. S.W. and E.S. were funded by Deutsche Forschungsgemeinschaft Grant WE2376/41.

1. Ahmad M, Cashmore AR (1993) *HY4* gene of *A. thaliana* encodes a protein with characteristics of a blue-light photoreceptor. *Nature* 366:162–166.
2. Chaves I, et al. (2011) The cryptochromes: Blue light photoreceptors in plants and animals. *Annu Rev Plant Biol* 62:335–364.
3. Weber S (2005) Light-driven enzymatic catalysis of DNA repair: A review of recent biophysical studies on photolyase. *Biochim Biophys Acta* 1707:1–23.
4. Sancar A (2008) Structure and function of photolyase and *in vivo* enzymology: 50th anniversary. *J Biol Chem* 283:32153–32157.

5. Ritz T, Adem S, Schulten K (2000) A model for photoreceptor-based magnetoreception in birds. *Biophys J* 78:707–718.
6. Schulten K, Swenberg CE, Weller A (1978) A biomagnetic sensory mechanism based on magnetic field modulated coherent electron spin motion. *Z Phys Chem NF* 111:1–5.
7. Rodgers CT (2009) Magnetic field effects in chemical systems. *Pure Appl Chem* 81:19–43.
8. Gindt YM, et al. (1999) Origin of the transient electron paramagnetic resonance signals in DNA photolyase. *Biochemistry* 38:3857–3866.
9. Giovani B, Byrdin M, Ahmad M, Brettel K (2003) Light-induced electron transfer in a cryptochrome blue-light photoreceptor. *Nat Struct Biol* 10:489–490.
10. Zeugner A, et al. (2005) Light-induced electron transfer in *Arabidopsis* cryptochrome-1 correlates with *in vivo* function. *J Biol Chem* 280:19437–19440.
11. Biskup T, et al. (2009) Direct observation of a photoinduced radical-pair intermediate in a cryptochrome DASH blue-light photoreceptor. *Angew Chem Int Ed* 48:404–407.
12. Banerjee R, et al. (2007) The signaling state of *Arabidopsis* cryptochrome 2 contains flavin semiquinone. *J Biol Chem* 282:14916–14922.
13. Bouly JP, et al. (2007) Cryptochrome blue light photoreceptors are activated through interconversion of flavin redox states. *J Biol Chem* 282:9383–9391.
14. Rodgers CT, Hore PJ (2009) Chemical magnetoreception in birds: A radical pair mechanism. *Proc Natl Acad Sci USA* 106:353–360.
15. Liedvogel M, Mouritsen H (2010) Cryptochromes—a potential magnetoreceptor: What do we know and what do we want to know? *J Roy Soc Interface* 7:S147–S162.
16. Ahlbom A, et al. (2000) A pooled analysis of magnetic fields and childhood leukaemia. *Brit J Cancer* 83:692–698.
17. Greenland S, et al. (2000) A pooled analysis of magnetic fields, wire codes, and childhood leukemia. *Epidemiology* 11:624–634.
18. International Agency for Research on Cancer (2002) *Static and extremely low-frequency (ELF) electric and magnetic fields. IARC monographs on the evaluation of carcinogenic risks to humans, vol. 80* (IARC, Lyon).
19. Advisory Group on Non-ionising Radiation (2001) AGNIR (2001) ELF electromagnetic fields and the risk of cancer. *Report of an Advisory Group on Non-ionising Radiation. Documents of the NRPB, Vol. 12* (National Radiological Protection Board, Chilton, Oxon, UK).
20. Reddy AB, Wong GKY, O'Neill J, Maywood ES, Hastings MH (2005) Circadian clocks: Neural and peripheral pacemakers that impact upon the cell division cycle. *Mutat Res* 574:76–91.
21. Timmel CR, Till U, Brocklehurst B, McLauchlan KA, Hore PJ (1998) Effects of weak magnetic fields on free radical recombination reactions. *Mol Phys* 95:71–89.
22. Lagroye I, Percherancier Y, Juutilainen J, Poulletier De Gannes F, Veyret B (2011) ELF magnetic fields: Animal studies, mechanisms of action. *Prog Biophys Mol Biol* 107:369–373.
23. Henbest KB, et al. (2008) Magnetic-field effect on the photoactivation reaction of *Escherichia coli* DNA photolyase. *Proc Natl Acad Sci USA* 105:14395–14399.
24. Langenbacher T, Immeln D, Dick B, Kottke T (2009) Microsecond light-induced proton transfer to flavin in the blue light sensor plant cryptochrome. *J Am Chem Soc* 131:14274–14280.
25. Aubert C, Mathis P, Eker APM, Brettel K (1999) Intraprotein electron transfer between tyrosine and tryptophan in DNA photolyase from *anacystis nidulans. Proc Natl Acad Sci USA* 96:5423–5427.
26. Popović DM, Zmiric A, Zaric SD, Knapp EW (2002) Energetics of radical transfer in DNA photolyase. *J Am Chem Soc* 124:3775–3782.
27. Weber S, et al. (2002) Photoactivation of the flavin cofactor in *Xenopus laevis* (6–4) photolyase: Observation of a transient tyrosyl radical by time-resolved electron paramagnetic resonance. *Proc Natl Acad Sci USA* 99:1319–1322.
28. Li YF, Heelis PF, Sancar A (1991) Active-site of DNA photolyase—tryptophan-306 is the intrinsic hydrogen-atom donor essential for flavin radical photoreduction and DNA-repair *in vitro. Biochemistry* 30:6322–6329.
29. Brettel K, Byrdin M (2010) Reaction mechanisms of DNA photolyase. *Curr Opin Struct Biol* 20:693–701.
30. Byrdin M, et al. (2004) Intraprotein electron transfer and proton dynamics during photoactivation of DNA photolyase from *E. coli*: Review and new insights from an "inverse" deuterium isotope effect. *Biochim Biophys Acta* 1655:64–70.
31. Weller A, Nolting F, Staerk H (1983) A quantitative interpretation of the magnetic-field effect on hyperfine-coupling-induced triplet formation from radical ion-pairs. *Chem Phys Lett* 96:24–27.
32. Miura T, Maeda K, Arai T (2006) The spin mixing process of a radical pair in low magnetic field observed by transient absorption detected nanosecond pulsed magnetic field effect. *J Phys Chem A* 110:4151–4156.
33. Shushin AI (1991) The effect of the spin exchange interaction on SNP and RYDMR spectra of geminate radical pairs. *Chem Phys Lett* 181:274–278.
34. Woiczikowski PB, Steinbrecher T, Kubar T, Elstner M (2011) Nonadiabatic QM/MM simulations of fast charge transfer in *Escherichia coli* DNA photolyase. *J Phys Chem B* 115:9846–9863.
35. Krapf S, Koslowski T, Steinbrecher T (2010) The thermodynamics of charge transfer in DNA photolyase: Using thermodynamic integration calculations to analyse the kinetics of electron transfer reactions. *Phys Chem Chem Phys* 12:9516–9525.
36. Efimova O, Hore PJ (2008) Role of exchange and dipolar interactions in the radical pair model of the avian magnetic compass. *Biophys J* 94:1565–1574.
37. Brautigam CA, et al. (2004) Structure of the photolyase-like domain of cryptochrome 1 from *Arabidopsis thaliana. Proc Natl Acad Sci USA* 101:12142–12147.
38. Eveson RW, Timmel CR, Brocklehurst B, Hore PJ, McLauchlan KA (2000) The effects of weak magnetic fields on radical recombination reactions in micelles. *Int J Radiat Biol* 76:1509–1522.
39. Brocklehurst B (1976) Spin correlation in geminate recombination of radical ions in hydrocarbons. 1. Theory of magnetic-field effect. *J Chem Soc Faraday Trans II* 72:1869–1884.
40. Kirschvink JL, Winklhofer M, Walker MM (2010) Biophysics of magnetic orientation: Strengthening the interface between theory and experimental design. *J R Soc Interface* 7:S179–S191.
41. Zuo Z, Liu H, Liu B, Liu X, Lin C (2011) Blue light-dependent interaction of CRY2 with SPA1 regulates COP1 activity and floral initiation in *Arabidopsis. Curr Biol* 21:841–847.
42. Liu B, Liu H, Zhong D, Lin C (2010) Searching for a photocycle of the cryptochrome photoreceptors. *Curr Opin Plant Biol* 13:578–586.
43. Partch CL, Sancar A (2005) Photochemistry and photobiology of cryptochrome blue-light photopigments: The search for a photocycle. *Photochem Photobiol* 81:1291–1304.
44. Bouly J, et al. (2003) Novel ATP-binding and autophosphorylation activity associated with *Arabidopsis* and human cryptochrome-1. *Eur J Biochem* 270:2921–2928.
45. Sang Y, et al. (2005) N-terminal domain-mediated homodimerization is required for photoreceptor activity of *Arabidopsis* cryptochrome 1. *Plant Cell* 17:1569–1584.
46. Kondoh M, et al. (2011) Light-induced conformational changes in full-length *Arabidopsis thaliana* cryptochrome. *J Mol Biol* 413:128–137.
47. Schleicher E, et al. (2005) Light-induced reactions of *Escherichia coli* DNA photolyase monitored by Fourier transform infrared spectroscopy. *FEBS J* 272:1855–1866.
48. Park H-W, Kim S-T, Sancar A, Deisenhofer J (1995) Crystal structure of DNA photolyase from *Escherichia coli. Science* 268:1866–1872.